Kovove Mater. 59 2021 231–236
DOI: 10.4149/km_2021_4_231

Observations on the intersection between $\{10\bar{1}1\}$ and $\{10\bar{1}2\}$ twin in deformed magnesium alloy

G. Xi[1]*, J. Zhang[2]**, J. Wu[1], J. Jia[1], Y. Zhi[1]

[1] *College of Material Science and Engineering, Chongqing University of Technology, Chongqing, 400054, P. R. China*
[2] *College of Materials Science and Engineering, Chongqing University, Chongqing 400044, P. R. China*

Received 30 April 2021, received in revised form 6 June 2021, accepted 8 June 2021

Abstract

Twin boundary plays a significant role in plastic deformation and consequently affects the mechanical properties of Mg alloys. In this work, the intersectant interfaces of $\{10\bar{1}1\}$-$\{10\bar{1}2\}$ double twin in deformed magnesium alloy were characterized employing high-resolution transmission electron microscopy (HRTEM). The result indicates that $\{10\bar{1}1\}$ twin boundary entirely departs from the theoretical twinning plane near the interaction site, while $\{10\bar{1}1\}$ plane of matrix and twin is parallel and $\{10\bar{1}1\}$ twin boundary is composed of $\{10\bar{1}1\}$ coherent twin boundary and $\{0002\} \parallel \{\bar{1}01\bar{1}\}$ basal-pyramidal (BPy) boundaries away from interaction site. Furthermore, the boundary interacted by $\{10\bar{1}1\}$ and $\{10\bar{1}2\}$ is decorated by BP/PB boundary, and $\{10\bar{1}2\}$-$\{10\bar{1}1\}$ twin interaction results in a high-angle asymmetrical tilt boundary at the interaction site. Correspondingly, the microstructural features related to the interactional incidents are discussed.

K e y w o r d s: Mg, twinning, twin-twin interaction, HRTEM

1. Introduction

Recently, magnesium (Mg) alloys have drawn interest for their potential application as structural components in the aerospace and automotive industries because of their outstanding properties, such as low density and high specific strength [1–3]. However, their widespread application has been limited because of their limited room temperature formability and strong directional anisotropy [4, 5]. As twinning for HCP-structured Mg can accommodate plastic strain along the *c*-axis and provide additional independent shear systems, it can play a vital role in determining the mechanical behavior, such as formability and strength of wrought Mg products [6, 7]. The twins in the deformed Mg alloys mainly include $\{10\bar{1}2\}$ tension twin and $\{10\bar{1}1\}$ compression twin [8]. Twin boundary often plays a significant role in plastic deformation and ultimately controls the mechanical properties of Mg and Mg alloys [9, 10]. Therefore, the interfacial structure of twin and twin-twin interactions has attracted much attention in recent years [11–15].

It is reported that the $\{10\bar{1}2\}$ twin boundary consists of $\{10\bar{1}2\}$ coherent twin boundary and basal-prismatic (BP/PB) boundary, and $\{10\bar{1}1\}$ twin boundary is composed of $\{10\bar{1}1\}$ coherent twin boundary, $\{0002\} \parallel \{\bar{1}01\bar{1}\}$basal-pyramidal (BPy) boundaries, $\{10\bar{1}1\} \parallel \{0002\}$ pyramidal-basal (PyB) boundaries and $\{10\bar{1}0\} \parallel \{10\bar{1}3\}$ prismatic-third pyramidal (P3Py) boundaries [16–19]. Recently, according to experimental observation and crystallographic analysis, Zhu et al. reported that the interaction between two co-zones $\{10\bar{1}2\}$ and $\{10\bar{1}1\}$ could result in tilt boundaries, with the boundary plane either basal-plane or prismatic-plane tilt about the $[1\bar{2}10]$ direction [20]. It should be noted that $\{10\bar{1}2\}$ twin can nucleate from $\{10\bar{1}1\}$ twin boundary when basal dislocations pile up and lead to stress concentration at one $\{10\bar{1}1\}$ twin boundary in our previous work [21]. After the $\{10\bar{1}2\}$ twin nucleates from one $\{10\bar{1}1\}$ twin boundary, it will grow up from $\{10\bar{1}1\}$ twin or matrix. If $\{10\bar{1}2\}$ twin grows up from $\{10\bar{1}1\}$ twin, it will interact with $\{10\bar{1}1\}$ twin. In this case, $\{10\bar{1}1\}$-$\{10\bar{1}2\}$ double twin will be formed and the $\{10\bar{1}1\}$ twin is a matrix of $\{10\bar{1}2\}$ twin [22, 23]. It should be noted that the voids and cracks are prone to form adjacent to the

*Corresponding author: e-mail address: gqxi@cqut.edu.cn
**Corresponding author: e-mail address: jingzhang@cqu.edu.cn

intersectant interfaces of $\{10\bar{1}1\}$-$\{10\bar{1}2\}$ double twin. However, until now, there has been little work on the structural feature of $\{10\bar{1}1\}$-$\{10\bar{1}2\}$ double twin and the interactional behavior of $\{10\bar{1}1\}$ twin and $\{10\bar{1}2\}$ twin, especially at an atomic scale.

It is the purpose of this study to apply transmission electron microscopy (TEM) and high-resolution TEM (HRTEM) to explore the structure when $\{10\bar{1}2\}$ twin interacts with $\{10\bar{1}1\}$ twin. The HRTEM observation shows that boundary interacted by $\{10\bar{1}2\}$ and $\{10\bar{1}1\}$ twin consists of BP/PB boundary and a high-angle asymmetrical tilt boundary from $\{10\bar{1}2\}$--$\{10\bar{1}1\}$ twin interaction at the interaction site. We find that $\{10\bar{1}1\}$ twin boundary deviates remarkably from the $\{10\bar{1}1\}$ plane, and the intersection angle between $\{10\bar{1}1\}$ planes of matrix and twin is measured to be $\sim 10°$ near the interaction site, while $\{10\bar{1}1\}$ plane of matrix and twin is parallel and $\{10\bar{1}1\}$ twin boundary is composed of $\{10\bar{1}1\}$ coherent twin boundary and $\{0002\} \parallel \{\bar{1}01\bar{1}\}$ basal-pyramidal (BPy) boundaries away from the interaction site. In view of this direct observation, the evolution of the twin boundary is discussed.

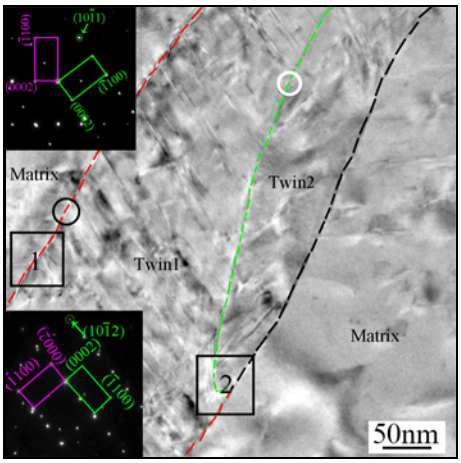

Fig. 1. Typical TEM morphology of $\{10\bar{1}1\}$-$\{10\bar{1}2\}$ twin interaction in deformed Mg alloy. Selected area electron diffractions inserted in the left upper corner and left lower corner confirm $\{10\bar{1}1\}$ and $\{10\bar{1}2\}$ twin orientation relationship, respectively. The electron beam is parallel to the $[1\bar{2}10]$ direction. The boundary interacted by $\{10\bar{1}1\}$ and $\{10\bar{1}2\}$ twin is marked by green lines.

2. Material and procedures

2.1. Material

A hot-rolled AZ31 (nominal composition Mg--3wt.%Al-1wt.%Zn) thick plate with a strong basal texture was used in this investigation.

2.2. Processing

The specimens with the dimensions 30 mm × 30 mm × 31 mm (*RD* × *TD* × *ND*) were machined from the center of rolled plate. Here, *RD*, *TD*, and *ND* refer to the rolling direction, transverse direction, and normal direction, respectively, of the initial plate. The compressive strain of 5.5 % in parallel to *RD* and re-compressive strain of 14.5 % in parallel to 45° of the *RD* and *ND* were applied to the block. The compression tests were carried out on a CMT6305-300 universal testing machine at a strain rate of $0.001\,s^{-1}$ at room temperature.

2.3. Microstructural characterization

For TEM analysis, a cross-sectional TEM specimen was taken from the deformed sample. Then, the samples for TEM and HRTEM observation were obtained by mechanical polishing and ion thinning using a precision ion polishing system (GATAN, PIPS II--691). Subsequently, the interfacial structure of $\{10\bar{1}1\}$--$\{10\bar{1}2\}$ double twin was examined with FEI Tecnai F20-G2 transmission electron microscope operating at 300 kV. The initial microstructure of the alloy and a more detailed description of the experimental process can be seen in our previous study [21].

3. Results

3.1. TEM observation

Figure 1 displays the typical bright-field TEM micrograph of deformed AZ31 alloy. Obviously, the twins are in contact with each other, and crossed twin patterns are formed in deformation microstructure. The twins are referred to as twin i ($i = 1, 2$). The red and green dashed lines represent the contours of twin 1 and twin 2. The selected area electron diffraction (SAED) pattern viewed along the $[1\bar{2}10]$ zone axis of the area as indicated by the black circle across the boundary (depicted by red dashed line) is inserted at the left upper corner. The mirror spots appear with respect to $\{10\bar{1}1\}$ planes, suggesting that twin 1 is regarded as $\{10\bar{1}1\}$ twinning orientation relationship. SAED pattern viewed along the $[1\bar{2}10]$ zone axis of the area as indicated by the white circle across the boundary (depicted by green dashed line) is inserted at the left lower corner. The figure shows that the mirror spots appear with respect to $\{10\bar{1}2\}$ planes, suggesting that twin 2 corresponds to $\{10\bar{1}2\}$ twin. It is interesting to note that $\{10\bar{1}1\}$ twin is a matrix of $\{10\bar{1}2\}$ twin, and the boundary between twin 1 and twin 2 is the $\{10\bar{1}2\}$ twin boundary. Furthermore, the boundary between twin 2 and the matrix of twin 1 is depicted by a black dashed line.

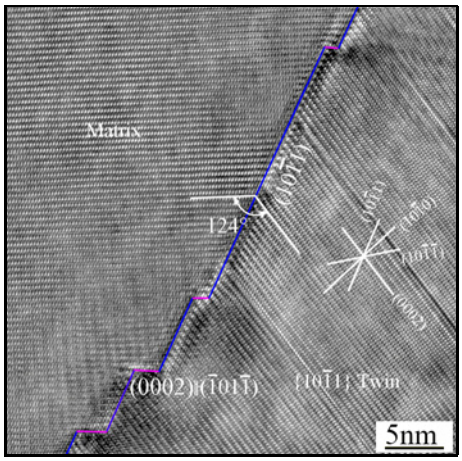

Fig. 2. High-resolution transmission electron microscopy showing microstructural features far away from the interaction site. The {10$\bar{1}$1} coherent boundaries are denoted by blue lines, and {0002} ∥ {10$\bar{1}$1} basal-pyramidal (BPy) boundaries are indicated by pink lines.

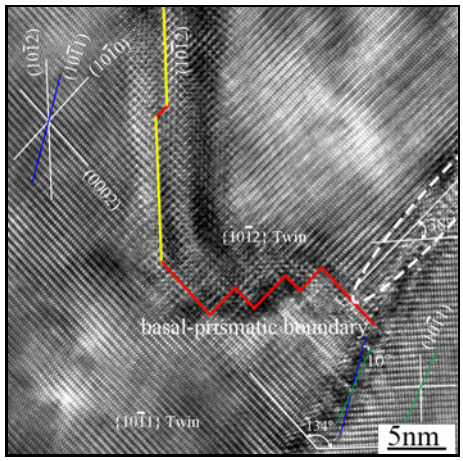

Fig. 3. High-resolution transmission electron microscopy showing microstructural features at interaction site. The {10$\bar{1}$2} coherent twin boundaries are marked by yellow lines, and BP/PB boundaries are colored in red.

3.2. HRTEM observations

To understand the boundary structure away from the interaction site, one region marked with black rectangular box 1 is selected to perform HRTEM characterization. The HRTEM image of position 1 is provided in Fig. 2. In this picture, the basal planes and the {10$\bar{1}$1} twin boundaries are edge-on since the image is taken along [1$\bar{2}$10] zone axis. The traces of (0002), {10$\bar{1}\bar{1}$}, {10$\bar{1}$1}, and {10$\bar{1}$0} planes of {10$\bar{1}$1} twin are displayed in the right lower corner. It can be seen that the twin boundary is incoherent and presents a faceted structure. The twin boundary contains straight terraces and a step-like interface. According to the orientation analysis, the straight terraces (depicted by solid blue lines) correspond to the theoretical {10$\bar{1}$1} coherent twin boundaries, while steps (depicted by solid pink lines) are parallel to {0002} ∥ {$\bar{1}$0$\bar{1}$1} boundaries. In this case, the misorientation between the basal planes of matrix and twin is theoretically 124°.

To understand the boundary structure at the interaction site, the other region marked with black rectangular box 2 is chosen to execute HRTEM observation. Figure 3 provides an HRTEM image of position 2. In the HRTEM image, the traces of (0002), {10$\bar{1}$1}, {10$\bar{1}$2}, and {10$\bar{1}$0} planes of {10$\bar{1}$1} twin and the traces of (0002), {10$\bar{1}$1} and {10$\bar{1}$0} planes of matrix are displayed in the left upper and right lower corner, respectively. It can be seen that the boundary between {10$\bar{1}$1} and {10$\bar{1}$2} twin is extremely incoherent and decorated by steps (indicated by solid red lines) at the interaction site. According to the orientation analysis, the steps are parallel to BP/PB boundaries. As can be seen, near the interaction site, the {10$\bar{1}$1} plane of {10$\bar{1}$1} twin and matrix is not parallel and included angle between {10$\bar{1}$1} plane of {10$\bar{1}$1} twin and matrix is 10°.

Moreover, the misorientation angle between the basal planes of {10$\bar{1}$1} twin and matrix is 134°, rather than theoretical 124°. This suggests that {10$\bar{1}$1} twin boundary deviates prominent from its theoretical twinning plane. It is worth noting that the atomic image is more blurred than those far away from the interaction site. This may be originated from the high lattice distortion stemming from local high-stress concentration, as reported by some previous studies [24–27]. In addition, the interaction between {10$\bar{1}$1} and {10$\bar{1}$2} results in a high-angle asymmetrical tilt boundary at the interaction site (marked with a white ellipse), and the misorientation angle is 38°.

4. Discussion

As mentioned above, the interfacial structure features significantly differ at the interaction site and away from the interaction site. Such structure features must influence the macroscopical performance of Mg alloys. Therefore, it is crucial to understand the underlying mechanism of the twin-twin interaction. It should be emphasized that deformation microstructure in the alloys was introduced by a 5.5 % *RD* pre-compression and a 14.5 % *RD* and *ND* 45° re-compression. {10$\bar{1}$1} twin first nucleates in the grain when the alloy is compressed along *RD*, and a number of basal dislocations would be activated in the matrix when re-compression along 45° of *RD* and *ND* is applied to the alloy, as demonstrated in a previous study [21].

Moreover, during the re-compression process, these

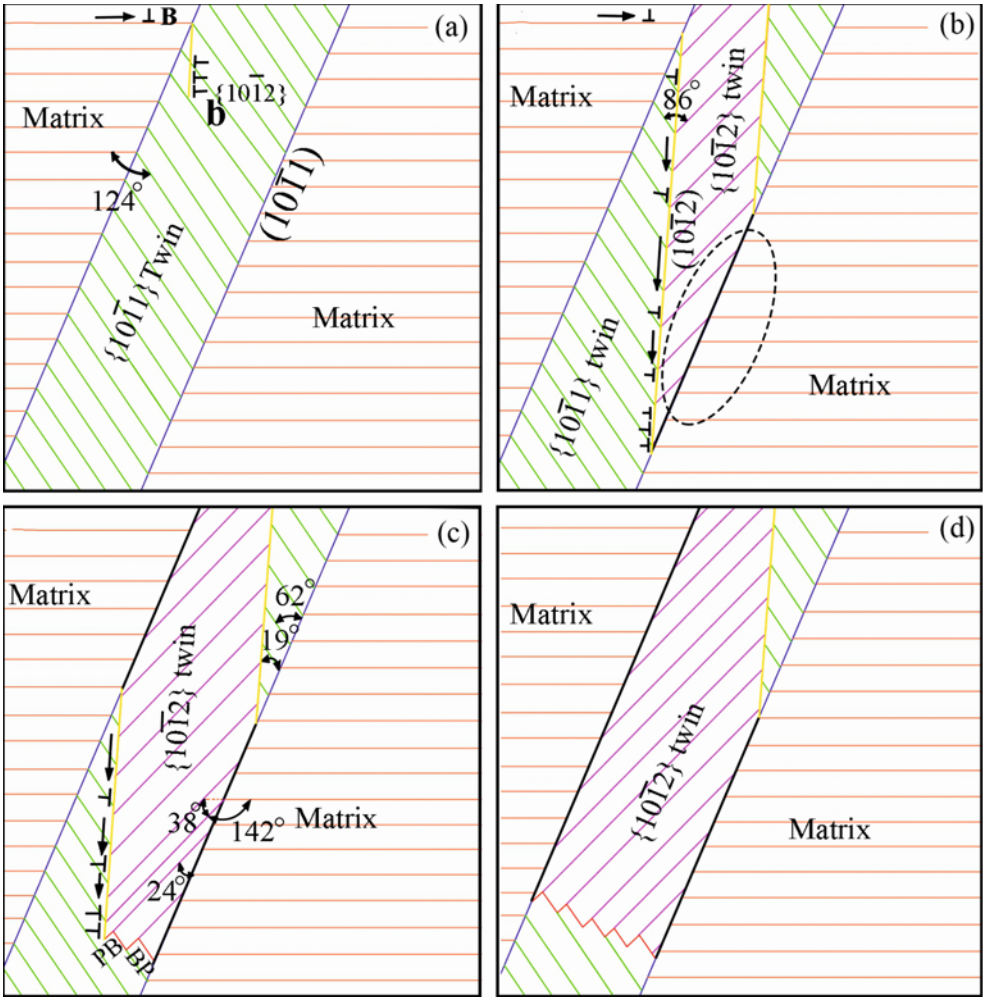

Fig. 4. Schematic diagram showing interaction process: {10$\bar{1}$1} twin boundaries are denoted by a solid blue line. The boundary interacted by {10$\bar{1}$1} and {10$\bar{1}$2} twin is colored by a yellow line. Capital letter "B" represents basal dislocation in the matrix and "b" represents {10$\bar{1}$2} twinning dislocation.

basal dislocations will interact with the {10$\bar{1}$1} twin boundaries. However, the number of dislocations that could be absorbed by {10$\bar{1}$1} twin boundary is limited. When the number of dislocations reaches the limit, a new {10$\bar{1}$2} twin nucleus can be formed in some position at one twin {10$\bar{1}$1} boundary due to differences in local stress [21, 28]. Then, it will grow up and interact with {10$\bar{1}$1} twin, since the migration of {10$\bar{1}$2} twin boundary is attributed to the gliding twinning dislocations [29, 30].

To better understand the {10$\bar{1}$1}-{10$\bar{1}$2} twin interaction and microstructural evolution, a schematic illustration of the interactional process is shown in Fig. 4. For simplicity, blue and yellow solid lines represent the incoherent {10$\bar{1}$1} twin boundary and the boundary between {10$\bar{1}$1} and {10$\bar{1}$2}, respectively. The basal planes of matrix, {10$\bar{1}$1} twin, and {10$\bar{1}$2} twin are denoted by brown, green, and pink solid lines. Herein, dislocations are denoted as "⊥" symbols, and their gliding directions are expressed by the black arrows. It can be seen in Fig. 4a because local stress is different; a new {1012} twin nucleates from {10$\bar{1}$1} twin boundary and serves to relax the stress concentration when the number of basal dislocations absorbed by the twin boundary reaches a certain threshold, as reported by previous research [21]. Accompanying the glide of the twinning dislocations along {10$\bar{1}$2} twin boundary, the twin grows up from {10$\bar{1}$1} twin and interacts with {10$\bar{1}$1} twin as depicted in Fig. 4b. At the interaction site, {10$\bar{1}$2} twinning dislocations will pile up because {10$\bar{1}$2} twinning dislocations glide are not favored at {10$\bar{1}$1} twin boundary. Therefore, it is concluded that BP/PB boundary will be formed due to the pile-up of {10$\bar{1}$2} twinning dislocations at the interaction site, and the {10$\bar{1}$2} twinning dislocations still pile up at the tip of {10$\bar{1}$2} the coherent twin boundary and BP/PB boundary as depicted in Fig. 4c. This is confirmed by the HRTEM image shown in Fig. 3. Meantime, it should be pointed out that {10$\bar{1}$2} nucleates from one {10$\bar{1}$1} twin bound-

ary located at the top left corner because local stress is different. However, the number of basal dislocations still pile up at the other $\{10\bar{1}1\}$ twin boundary located at the lower right corner of the image. Therefore, the large deviation of $\{10\bar{1}1\}$ twin boundary from $\{10\bar{1}1\}$ twinning plane results from an accommodation of strain near the interaction site. In addition, it should be mentioned that the interaction between $\{10\bar{1}2\}$ and $\{10\bar{1}1\}$ twin results in a high-angle asymmetrical tilt boundary at the interaction site (denoted by a solid black line). The misorientation angle between the basal planes across the tilt boundary is 38°, which is consistent with the experimental image in Fig. 3. Upon further strain, more BP/PB boundaries are formed at the tip, result in boundary between $\{10\bar{1}2\}$ and $\{10\bar{1}1\}$ decorated by BP/PB boundaries, and it is approximately perpendicular to $\{10\bar{1}1\}$ twin boundary, as depicted in Fig. 4d. This implies that $\{10\bar{1}2\}$ twin does not consume $\{10\bar{1}1\}$ twin upon further strain, which may result in the voids and cracks adjacent to the intersectant interfaces.

5. Conclusions

In summary, the interactions between $\{10\bar{1}2\}$ and $\{10\bar{1}1\}$ twin in AZ31 Mg alloy have been investigated by TEM and HRTEM, revealing the microstructural features at the interaction site and away from the interaction site. The main conclusions can be drawn as follows:

1. $\{10\bar{1}1\}$ twin boundary consists of $\{10\bar{1}1\}$ coherent twin boundary and $\{0002\} \parallel \{\bar{1}01\bar{1}\}$ boundaries away from interaction site. In addition, the misorientation angle between the basal planes of twin and matrix is theoretical 124° away from the interaction site.

2. Boundary between $\{10\bar{1}2\}$ and $\{10\bar{1}1\}$ is decorated by BP/PB boundary at the interaction site, and actual $\{10\bar{1}1\}$ twin boundary can deviate remarkably from the $\{10\bar{1}1\}$ plane by about 10° near the interaction site. Moreover, the significant deviation is proposed to result from strain accommodation.

3. $\{10\bar{1}2\}$-$\{10\bar{1}1\}$ twin interaction results in a high-angle asymmetrical tilt boundary at the interaction site, and the misorientation angle across the tilt boundary is 38°. Furthermore, it is proposed that the boundary between $\{10\bar{1}2\}$ and $\{10\bar{1}1\}$ decorated by BP/PB boundaries is approximately perpendicular to $\{10\bar{1}1\}$ twin boundary upon the further strain.

Acknowledgements

This work was supported by the Key Research and Development Program of Guangdong Province (2020B010186002); the Science and Technology Research Program of Chongqing Municipal Education Commission (KJQN202001106); the Scientific Research Foundation of Chongqing University of Technology (2019ZD32), and the University Innovation Research Group of Chongqing (CXQT20023).

References

[1] S. R. Agnew, J. F. Nie, Preface to the viewpoint set on: The current state of magnesium alloy science and technology, Scripta Mater. 63 (2010) 671–673. doi:10.1016/j.scriptamat.2010.06.029

[2] Z. X. Wu, W. A. Curtin, The origins of high hardening and low ductility in magnesium, Nature 526 (2015) 62–67. doi:10.1038/nature15364

[3] R. Chen, S. Sandlöbes, C. Zehnder, X. Q. Zeng, S. Korte-Kerzel, D. Raabe, Deformation mechanisms, activated slip systems and critical resolved shear stresses in an Mg-LPSO alloy studied by micropillar compression, Mater. Des. 154 (2018) 203–216. doi:10.1016/j.matdes.2018.05.037

[4] J. Zhang, M. Liu, Y. C. Dou, G. B. Liu, Role of alloying elements in the mechanical behaviors of an Mg-Zn--Zr-Er alloy, Metall. Mater. Trans. A 45 (2014) 5499–5507. doi:10.1007/s11661-014-2526-4

[5] H. Zhang, Y. C. Zhao, Y. Yan, J. F. Fan, L. F. Wang, H. B. Dong, B. S. Xu, Microstructure evolution and mechanical properties of Mg matrix composites reinforced with Al and nano SiC particles using spark plasma sintering followed by hot extrusion, J. Alloys Compd. 725 (2017) 652–664. doi:10.1016/j.jallcom.2017.07.159

[6] F. L. Wang, C. D. Barrett, R. J. McCabe, H. El Kadiri, L. Capolungo, S. R. Angew, Dislocation induced twin growth and formation of basal stacking faults in $\{10\bar{1}2\}$ twins in pure Mg, Acta Mater. 165 (2019) 471–485. doi:10.1016/j.actamat.2018.12.003

[7] C. D. Barrett, H. El Kadiri, The roles of grain boundary dislocations and disclinations in the nucleation of $\{10\bar{1}2\}$ twinning, Acta Mater. 63 (2014) 1–15. doi:10.1016/j.actamat.2013.09.012

[8] B. Song, Q. S. Yang, T. Zhou, L. J. Chai, N. Guo, T. T. Liu, S. F. Guo, R. L. Xin, Texture control by $\{10\bar{1}2\}$ twinning to improve the formability of Mg alloys: A review, Journal of Materials Science & Technology 35 (2019) 2269–2282. doi:10.1016/j.jmst.2019.03.045

[9] H. Zhang, M. X. Yang, M. J. Hou, L. F. Wang, Q. Zhang, J. F. Fan, W. G. Li, H. B. Dong, S. M. Liu, B. S. Xu, Effect of pre-existing $\{10\bar{1}2\}$ extension twins on mechanical properties, microstructure evolution and dynamic recrystallization of AZ31 Mg alloy during uniaxial compression, Mater. Sci. Eng. A 744 (2019) 456–470. doi:10.1016/j.msea.2018.11.146

[10] Q. Sun, A. Ostapovets, X. Y. Zhang, L. Tan, Q. Liu, Investigation of twin-twin interaction in deformed magnesium alloy, Philos. Mag. 98 (2018) 741–751. doi:10.1080/14786435.2017.1417648

[11] Y. M. Zhu, S. W. Xu, J. F. Nie, $\{10\bar{1}1\}$ twin boundary structures in an Mg-Gd alloy, Acta Mater. 143 (2018) 1–12. doi:10.1016/j.actamat.2017.09.067

[12] H. El Kadiri, J. Kapil, A. L. Oppedal, S. R. Agnew, M. Cherkaoui, S. C. Vogel, The effect of twin-twin interactions on the nucleation and propagation of $\{10\bar{1}2\}$

twinning in magnesium, Acta Mater. 61 (2013) 2549–3563. doi:10.1016/j.actamat.2013.02.030
[13] M. Arul Kumar, M. Gong, I. J. Beyerlein, J. Wang, C. N. Tomé, Role of local stresses on co-zone twin-twin junction formation in HCP magnesium, Acta Mater. 158 (2019) 353–361. doi:10.1016/j.actamat.2019.02.037
[14] F. Mokdad, D. L. Chen, D. Y. Li, Twin-twin interactions and contraction twin formation in an extruded magnesium alloy subjected to an alteration of compressive direction, J. Alloys Compd. 737 (2018) 549–560. doi:10.1016/j.jallcom.2017.12.043
[15] Q. Yu, J. Wang, Y. Y. Jiang, R. J. McCabe, N. Li, C. N. Tomé, Twin-twin interactions in magnesium, Acta Mater. 77 (2014) 28–42. doi:10.1016/j.actamat.2014.05.030
[16] J. Zhang, G. Q. Xi, X. Wan, C. Fang, The dislocation--twin interaction and evolution of twin boundary in AZ31 Mg alloy, Acta Mater. 133 (2017) 208–216. doi:10.1016/j.actamat.2017.05.034
[17] M. Gong, S. Xu, Y. Y. Jiang, Y. Liu, J. Wang, Structural characteristics of $\{10\bar{1}2\}$ non-co-zone twin-twin interactions in magnesium, Acta Materialia 159 (2018) 65–76. doi:10.1016/j.actamat.2018.08.004
[18] A. Ostapovets, A. Serra, Characterization of the matrix-twin interface of a $\{10\bar{1}2\}$ twin during growth, Philos. Mag. 94 (2014) 2827–2839. doi:10.1080/14786435.2014.933906
[19] A. Ostapovets, R. Gröger, Twinning disconnections and basal-prismatic twin boundary in magnesium, Model. Simul. Mater. Sci. 22 (2014) 055007–055020. doi:10.1088/0965-0393/22/2/025015
[20] Y. M. Zhu, M. Z. Bian, J. F. Nie, Tilt boundaries and associated solute segregation in an Mg-Gd alloy, Acta Mater. 127 (2017) 505–518. doi:10.1016/j.actamat.2016.12.032
[21] J. Zhang, G. Q. Xi, X. Wan, $\{10\bar{1}1\}$ twin boundary showing very large deviation from the theoretical one in deformed magnesium alloy, Mater. Charact. 132 (2017) 280–283. doi:10.1016/j.matchar.2017.08.021
[22] A. G. Crocker, Double twinning, Philosophical Magazine 7 (1962) 1901–1924. doi:10.1080/14786436208213854
[23] A. Dubertret, A. Le Lann, Development of a new model for atom movement in twinning. Case of the {1011}, {1013} twins and {1011}, {1012} double twinning in H.C.P. metals, Physica Status Solidi A 60 (1980) 141–145. doi:10.1002/pssa.2210600118
[24] F. Wu, H. M. Wen, E. J. Lavernia, J. Narayan, Y. T. Zhu, Twin intersection mechanisms in nanocrystalline fcc metals, Mater. Sci. Eng. A 585 (2013) 292–296. doi:10.1016/j.msea.2013.07.063
[25] H. Li, X. J. Xu, Q. Sun, X. Y. Zhang, X. Y. Fang, M. H. Zhu, Investigation of interfacial feature and interactional behavior of $\{11\bar{2}2\}$ twin in deformed titanium, J. Alloys Compd. 788 (2019) 1137–1145. doi:10.1016/j.jallcom.2019.02.309
[26] M.Y. Gong, S. Xu, Y. Y. Jiang, Y. Liu, J. Wang, Structural characteristics of non-$\{10\bar{1}2\}$ co-zone twin-twin interactions in magnesium, Acta Mater. 159 (2018) 65–76. doi:10.1016/j.actamat.2018.08.004
[27] H. El Kadiri, J. Kapil, A. L. Oppedal, L. G. Hector Jr., S. R. Agnew, M. Cherkaoui, S. C.Vogelf, The effect of twin-twin interactions on the nucleation and propagation of $\{10\bar{1}2\}$ twinning in magnesium, Acta Mater. 61 (2013) 3549–3563. doi:10.1016/j.actamat.2013.02.030
[28] I. J. Beyerlein, J. Wang, M. R. Barnett, C. N. Tomé, Double twinning mechanisms in magnesium alloys via dissociation of lattice dislocations, Proc. R. Soc. A 468 (2012) 1496–1520. doi:10.2307/41511074
[29] M. J. Hao, W. L. Cheng, L. F. Wang, E. Mostaed, L. P. Bian, H. X. Wang, X. F. Niu, Texture evolution in Mg-8Sn-1Zn-1Al alloy during hot compression via competition between twinning and dynamic precipitation, Mater. Sci. Eng. A 748 (2019) 418–427. doi:10.1016/j.msea.2019.01.108
[30] X. Y. Shi, A. A. Luo, S. C. Sutton, L. Zeng, S. Y. Wang, X. Q. Zeng, D. J. Li, W. J. Ding, Twinning behavior and lattice rotation in an Mg-Gd-Y-Zr alloy under ballistic impact, J. Alloys Compd. 650 (2015) 622–632. doi:10.1016/j.jallcom.2015.08.020